Temperature rise due to fast-moving dislocations

de Hosson, J.T.M.; Roos, A; Metselaar, E.D.

Published in:
Philosophical Magazine A-Physics of Condensed Matter Structure Defects and Mechanical Properties

DOI:
10.1080/01418610108214431

Publication date:
2001

PHILOSOPHICAL MAGAZINE A, 2001, VOL. 81, NO. 5, 1099–1120

Temperature rise due to fast-moving dislocations

J. TH. M. DE HOSSON†, A. ROOS and E. D. METSELAAR

Department of Applied Physics, Materials Science Center and Netherlands Institute for Metals Research, University of Groningen, Nijenborgh 4, 9747 AG Groningen, The Netherlands

[*Received 27 March 2000 and accepted 12 June 2000*]

ABSTRACT

In this paper, the method of discrete dislocation plasticity (DDP) is extended to include explicitly the thermal effects of moving dislocations. In this manner, localization of heat during fast deformation can be calculated exactly. The thermal effects included are the thermal dissipation due to dislocation drag, the temperature dependence of the drag coefficients themselves and a temperature-dependent obstacle strength through a simple Arrhenius-type dependence. An analytical solution is presented and the temperature distribution is calculated using a time-dependent Galerkin finite-element solution. The two solutions are compared to provide a mutual validation. Then, the stress–strain curves are calculated for Al under simple shear for constant temperatures of 100, 298 and 900 K. The stress–strain curves reflect the temperature dependence of the drag coefficients, since the deformation takes place at a strain rate of $10^6\,s^{-1}$, which is well within the drag-controlled regime. Finally, the temperature distributions for Al and Ti are calculated. At 7.5% shear strain, the maximum temperature rise is of the order of 20 K in Ti. This is orders of magnitude lower than the melting temperature, the temperature which has experimentally observed to be reached. It is anticipated that this is caused by crack propagation which will be modelled by a DDP approach in future work.

§1. INTRODUCTION

A prominent contribution to the field of dislocation dynamics was made by introducing the computer as an aid to clarify many phenomena that were not always experimentally accessible, such as the structure of dislocation cores and the motion of the dislocations. Mike Duesbery was a world-known expert in this area and his seminal work stimulated many investigations over the last decades, clarifying structural aspects related to plasticity in metallic systems. Through these studies, our understanding of the role of dislocations became more satisfactory and new concepts were further developed (Duesbery 1989).

In recent years, numerical algorithms have become increasingly sophisticated. Besides dislocation-core structure calculations (Vitek 1974), computational techniques such as the *ab-initio* calculations, Monte Carlo method, molecular dynamics (MD) and finite elements have found widespread use in many branches of materials science and engineering. However, even at the current rate of increase in number-crunching power, it is recognized that it will not be possible in the fore-

† Email: hossonj@phys.rug.nl

Philosophical Magazine A ISSN 0141–8610 print/ISSN 1460-6992 online © 2001 Taylor & Francis Ltd
http://www.tandf.co.uk/journals
DOI: 10.1080/01418610110033975

seeable future to simulate the deformation of a macroscopic workpiece directly from the motion of atoms around dislocation cores. It is therefore necessary to split up the important processes according to the time and length scales in which they play a significant role (Kirchner *et al.* 1996). The processes taking place on the smaller scale then give rise to a certain effective behaviour on a larger scale. For instance, the atomic configuration around a dislocation core (Vitek 1974) directly affects its scattering of lattice waves, thereby contributing to the drag force. On the other hand, when calculating the dislocation velocity due to the resolved shear stress, only this drag force is important, and not so much the precise atomic arrangement.

The connection between different length scales is not always easily made. For a discussion on length scale effects in relation to mechanical stresses, reference is made to Horstemeyer and Baskes (1999). For instance, in many engineering calculations of plastic deformation, the material is considered to be a continuum. In those cases, the relation between macroscopic stress and macroscopic strain (the constitutive relation) is specified, usually without taking into account the discrete nature of the carriers of plastic flow, namely the dislocations. This approach is successful for some applications, but it has the disadvantage that the material behaviour for each type of deformation has to be known in advance, which is not always the case.

On the other hand, some approaches exist nowadays that do take into account underlying microstructural processes. One such method is based on the so-called discrete dislocation plasticity (DDP) and calculates the deformation of a two-dimensional computational cell by considering the long-range stresses and displacements of edge dislocations moving under influence of an externally applied deformation rate (Van der Giessen and Needleman 1995). One area where this approach is particularly interesting is in the regime of very fast deformation. Measurements at high deformation rates are particularly difficult to perform. The deformation is often localized in very small volumes in which the temperature rises considerably during the process, sometimes even melting the material. Recrystallization due the temperature rise destroys most of the information of the processes preceding it. For these reasons the constitutive equations necessary in engineering calculations are often unreliable.

This paper approaches fast deformation from the small length scale. Specifically, it focuses on the processes taking place on a single slip system in a single grain of close-packed metal, where the emphasis lies on the fact that the deformation takes place in a very short time span and at very high rates. It is interesting to note that recently, based on MD simulations of twinning from the crack tip, Cerv *et al.* (2000) concluded that even a constant transonic velocity of twin extension is possible in narrow stress intervals in bcc Fe at velocities of 4000–5000 $\mathrm{m\,s^{-1}}$. One extension of DDP is to take into account the limiting velocity to dislocation motion, which is the velocity of sound (Mason *et al.* 1994). This implies taking into account the velocity dependence of the displacement and stress fields of a moving dislocation in a drag-controlled regime (Metselaar *et al.* 1999, Roos *et al.* 1998).

In this paper the DDP methodology is extended further to calculate explicitly the localization of heat and its effects on the strengths of obstacles and drag forces. In the past, some estimates of the maximum temperature rise due to plastic flow have been made in the literature, but it has never been calculated exactly. During fast deformation, a vast amount of energy (in the form of mechanical work) is put into the material during a relatively short period of time (Roos *et al.* 2000). Through the damping of dislocation motion by electrons and phonons (Roos and De Hosson 2001) the kinetic energy of a dislocation is dissipated into heat. The resulting tem-

perature rise may have considerable effects on certain microstructural processes. For instance, thermally assisted passing of obstacles by a dislocation is greatly facilitated, thereby effectively lowering the flow stress. On the other hand, the viscous damping of dislocation motion increases owing to increased lattice vibrations. Another parameter, the mobility of point defects (for instance vacancies and interstitials), also depends critically on temperature and the production rate of point defects by moving dislocations (Detemple *et al.* 1995). When the processing time is short, the heat may not have sufficient time to become dissipated throughout the workpiece or radiated into the environment. Locally, the temperature may become very high. For instance, Coffey (1984) found droplets of previously molten Ti on the surface of a shear plug of Ti_6Al_4V. Evidently, because of fracture the local temperature must have risen as high as the melting point of Ti, which is of the order of 1650°C.

A measure of the extent of the region through which the heat is dissipated during a time increment k of duration $\Delta t_k \equiv t_{k+1} - t_k$ is the thermal diffusion length (Carslaw and Jäger 1959). It is specified in terms of the thermal conductivity K, the material density ρ and the specific heat c:

$$\ell_k = 2\left(\frac{K}{\rho c}\,\Delta t_k\right)^{1/2} \equiv 2(\kappa \Delta t_k)^{1/2}, \tag{1}$$

with κ the thermal diffusivity. Table 1 lists the thermal diffusion length for the range of duration of the time increments occurring in the simulations of high-strain-rate deformation using the method of DDP (Roos *et al.* 2000). It can be seen that, typically, the heat front travels some tens of Burgers vectors during one time increment.

In the literature, a few discussions about the temperature rise due to moving dislocation can be found. Among the first to discuss the heating effect of moving dislocations were Freudenthal and Weiner (1956) and, subsequently, Eshelby and Pratt (1956). Their discussion suggested that ordinary motion of dislocation on their slip plane will cause a temperature rise of at most a few tens of kelvins. Depending on a parameter $\Lambda = 2\kappa/v$, they predicted an upper limit for the temperature rise ΔT of

$$\Delta T_{MAX} \leqslant \begin{cases} n\,\dfrac{\sigma_{PK} b v}{2K} \ln\left(\dfrac{n\Lambda}{\lambda}\right) & \text{for} \quad \Lambda \gg \lambda, \\ n\,\dfrac{\sigma_{PK} b v}{2K}\left(\dfrac{\Lambda}{\lambda}\right)^{1/2} & \text{for} \quad \Lambda \ll \lambda, \end{cases} \tag{2}$$

where n denotes the number of dislocations with a Burgers vector of magnitude b running with velocity v on the slip plane spread over a distance λ under the influence by the resolved (Peach–Koehler) shear stress σ_{PK}. Using n = 500 dislocations and

Table 1. Thermal diffusion length λ_k for typical time increments Δt_k (Weast *et al.* 1984).

	κ (at 298 K)	b	ℓ_k/b		
	$(10^{-6}\,m^2\,s^{-1})$	(nm)	$\Delta t_k = 10^{-13}$ s	$\Delta t_k = 10^{-11}$ s	$\Delta t_k = 10^{-9}$ s
Ti	6.7	0.2910	6	56	561
Al	48.3	0.2862	15	154	1535
Cu	116.1	0.2556	27	267	2667

$\lambda \approx 10^{-3}$ m for well annealed Al, they predicted a temperature rise of about 0.5 K. They concluded that a large temperature rise can only occur if the dislocations are very closely packed and then suddenly released, or at very high loading rates.

Armstrong and Elba (1989) pointed out that at high loading rates, where the deformation is localized in adiabatic slip bands, the small volume in which the deformation takes place, takes an increasingly important role. In contrast, the previous models averaged the temperature over a larger volume. They also worked out the conditions under which a static pile-up of dislocations breaks down through an obstacle to give a catastrophic pile-up avalanche. The energy that is stored in the configuration of the pile-up is then released suddenly, and, owing to the local nature of this event, the temperature rise may be orders of magnitude higher than predicted by the previous models. The upper limit for the temperature rise ΔT_{max} (i.e. when the concentrated shear stress at the tip of the pile-up reaches the fracture stress of the order of $\pi\mu(1-\nu)/8(2-\nu)$) is

$$\Delta T \leqslant \begin{cases} \dfrac{k_s d^{1/2} v}{16\pi K} \ln\left(\dfrac{\Lambda}{b}\right) & \text{for} \quad \Lambda > b \\ \dfrac{k_s d^{1/2} v}{16\pi K} \left(\dfrac{\Lambda}{b}\right)^{1/2} & \text{for} \quad \Lambda \leqslant b, \end{cases} \tag{3}$$

with k_s the microstructural shear stress intensity factor for the pile-up and d the average grain diameter. Using the parameters $k_s = 14\,\mathrm{N\,mm^{-3/2}}$, $d = 1$ mm and $v = a_1$ (the longitudinal wave velocity), $\Delta T_{max} = 2.3 \times 10^4$ K for Al. Similarly, in Ti, with $k_s = 21\,\mathrm{N\,mm^{-3/2}}$, $\Delta T_{max} = 3.2 \times 10^5$ K.

It is also of interest to note that the temperature field that is used in the derivations is essentially for $\Delta t_k \to \infty$, even though Armstrong and Elba (1989) took the effect of the sudden temperature rise into account through the reduced volume of the slip band. However, this paper extends the method of discrete dislocation plasticity to incorporate explicitly the kinetic temperature field resulting from the movement of individual dislocations. The advantage is that no assumptions have to be made about spacing of dislocations, lengths of pile-ups, stress concentration factors etc., because these parameters follow automatically from the formalism of discrete dislocation plasticity.

§ 2. Thermal effects on microstructural parameters

The temperature rise directly affects a number of microstructural parameters, although the dependence varies with the underlying physical mechanism. Depending on whether the deformation takes place in the regime of jerky glide or drag-controlled flow, thermal effects that manifest themselves in the overall deformation behaviour result from reductions in the effective obstacle strengths, or a temperature-dependent drag coefficient. The latter was treated elsewhere (Roos and De Hosson 2001). The elastic coefficients and corresponding Poisson's ratio also depend on temperature, but the dependence is usually taken to be weak and will be neglected. However, it should be realized that the elastic constants are directly related to the phonon spectra. The fact that elastic constants have self-averaging properties on a larger scale does not automatically apply on the local scale of the few Burgers vectors of the fast-moving dislocation acting as a heat source. Nevertheless, to a first approximation we assume that the phonon distribution is, on average, equal

to the distribution in thermal equilibrium and consequently the elastic constants themselves do not change.

In particular this paper deals with the so-called drag-controlled regime, that is at higher strain rates where thermal activation is not rate controlling. An estimate of the strain rates at which this transition occurs can be made as follows. In the thermally activated regime the effective barrier height for dislocation motion can be lowered by an amount ΔG provided by thermal fluctuations. When the dislocation segment vibrates with a frequency of ν_D, the rate at which obstacles are overcome by thermal fluctuations is given by the Arrhenius term $\nu_D \exp(-\Delta G/k_B T)$. Typically, the attack frequency ν_D lies in the range 10^9- $10^{11}\,s^{-1}$, depending on the length of the dislocation line segment. ΔG effectively increases with increasing temperature but decreases with increasing strain rate. The effect of the thermal energy is to decrease the height of the barrier, lowering the obstacle strength to an effective obstacle strength. However, as the strain rate increases, there is less time available to overcome the barrier until, at a critical strain rate $\dot{\gamma}_0$, the thermal activation is rendered ineffective, and an effective applied stress equal to the full obstacle strength has to be provided to overcome the obstacle. Although all activation events have the same probabilities of overcoming the obstacle, there are fewer activation events. This has the same effect as a stronger obstacle at a lower strain rate, or as a lower temperature. A simple estimate of the critical strain rate is setting the rate v/b at which the dislocation passes the Peierls hills equal to the attack frequency ν_D, and with an estimate of the mobile dislocation density (De Hosson *et al.* 1983):

$$\dot{\gamma}_0 = \nu_D \rho_{RUN} b^2 \approx \frac{\nu_D \rho_{TOT} b^2}{4}. \tag{4}$$

For a dislocation density $\rho_{TOT} = 10^{12} - 10^{14}\,m^{-2}$, the critical strain rate is of the order 10^3- $10^5\,s^{-1}$. At higher strain rates, the effect of temperature is determined by the temperature dependence of the drag coefficient.

The temperature dependence of the drag coefficients consisting of electron viscosity and phonon viscosity is dominated by the phonon contribution. The terms contributing to phonon damping may be grouped according to whether the dislocation line is considered flexible or rigid. In the first case, the thermal phonons excite vibrations in the dislocation line, which are then reradiated in a cylindrical wave around the dislocation line. When the dislocation is moving, this gives rise to a net force opposing the motion. This is called the flutter mechanism and it is described in terms of linear elasticity by B_{flut} (Kogure and Hiki 1975). In the second group, where the dislocation is considered rigid, it cannot scatter phonons by fluttering. However, close to the dislocation core, linear elasticity ceases to be valid, and the phonons are scattered by anharmonicities in the strain field. A moving dislocation encounters more phonons in the direction of motion than in other directions (giving rise to the so-called phonon wind), and the resulting drag coefficient is called B_{wind} (Nadgornyi 1988). At low temperatures, it is proportional to T^5 while, at high temperatures, $B_{wind} \propto T$ (as in the case of the flutter mechanism).

In the following we are focusing on the velocity dependence and we assume that only B_{flut} is velocity dependent. The velocity dependence and T dependence of the electron drag coefficients can be neglected. For intermediate to high temperatures (say $\Theta_D/3 < T < 3\Theta_D$, with Θ_D the Debye temperature) the total drag coefficient becomes (Roos and De Hosson 2001):

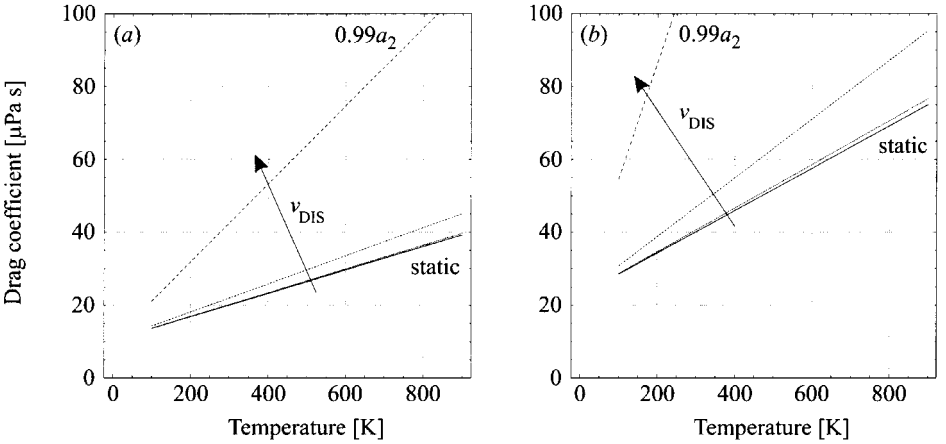

Figure 1. Temperature dependence of the drag coefficient $B_{TOT}(v, T)$ for (*a*) Cu and (*b*) Al: (——), static value; (· · · · · ·), v = 0.50a$_2$; (- - - -), v= 0.90a_2; (— — — — — — — —),v= 0.99a_2.

$$B_{TOT}(v, T) = \left(B^0_{wind}(\Theta_D) + \frac{B^0_{flut}(\Theta_D)}{1 - (v/a_2)^2} \right) \frac{T}{\Theta_D}, \tag{5}$$

where a_2 is the shear wave velocity. The ratios of the various contributions at the Debye temperature can be found using the equations given by Roos and De Hosson (2001) and the experimental values. Some values are plotted in figure 1 for Cu and Al.

§ 3. Heat equation

The heat transport equations are developed in a Cartesian (x_1, x_2, x_3) laboratory reference frame. The computational cell is depicted in figure 2. The energy balance of an infinitesimal volume element at a point P at (x_1, x_2, x_3) yields

$$\nabla \cdot [K(T)\nabla T] + \dot{q}_v = \rho(T) c_v(T) \frac{\partial T}{\partial t}, \tag{6}$$

where $\dot{q}_v$ represents the rate of heat generation of a heat source present in the volume, $\rho(T)$ represents the material density and $c_v(T)$ is the specific heat at constant volume. In the following, the heat conductivity, the specific heat and the material density are assumed to be independent of temperature. This assumption may not hold for cases when the local temperature rise is of the order of a few hundred kelvins or when the phonon distribution is not in equilibrium locally, but for now, we shall retain it. The heat equation then reduces to

$$\nabla^2 T + \frac{\dot{q}_v}{K} = \frac{\rho c_v}{K} \frac{\partial T}{\partial t} \equiv \frac{1}{\kappa} \frac{\partial T}{\partial t}. \tag{7}$$

Consider a straight dislocation moving in the computational cell with velocity v in the x_1 direction under the influence of the resolved shear stress σ_{PK} (Burgers vector of length b oriented in the x_1 direction; dislocation line along the x_3 direction). Owing to the damping of the dislocation motion, it acts as a moving line source of heat (which we shall denote by q_k during time increment k, to distinguish it from

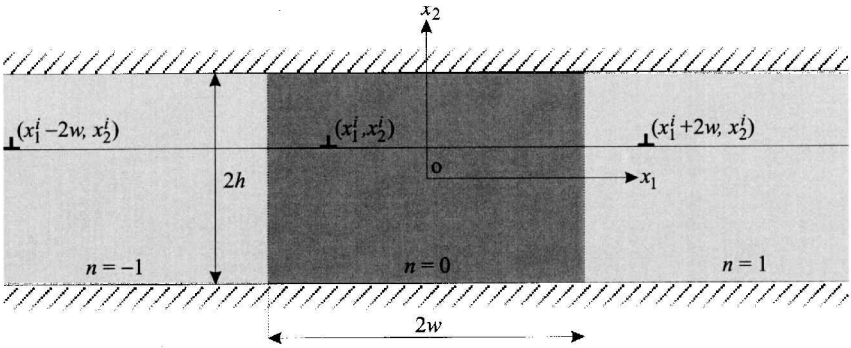

Figure 2. Computational cell ($n = 0$) of width × height = $2w \times 2h$ containing dislocation i at (x_1^i, x_2^i). Replicas of dislocation i are shown in the periodic neighbouring cells $n = -1$ and $n = 1$. The thermal boundary conditions are also shown, where in our case $dT/dx_2 = 0$ at $x_2 = \pm h$.

the volume source q_v). Per unit line length a quantity of heat is emitted at a rate of (Eshelby and Pratt 1956)

$$\dot{q}_k = b\sigma_{PK}v, \tag{8}$$

where it is understood that σ_{PK} and v also have their values of time increment k; in the method of DDP the dislocation velocity v and the resolved shear stress are piecewise constant functions of time.

In another paper (Roos and De Hosson 2001) we argued that the velocity-dependent contribution to the phonon drag B_{PH}, due to the flutter mechanism, can be found by taking the Fourier transform of the velocity-dependent strain fields (Gruner, 1965, Metselaar *et al.* 1999, Roos *et al.* 1998). In the case of an edge dislocation the relevant contribution is

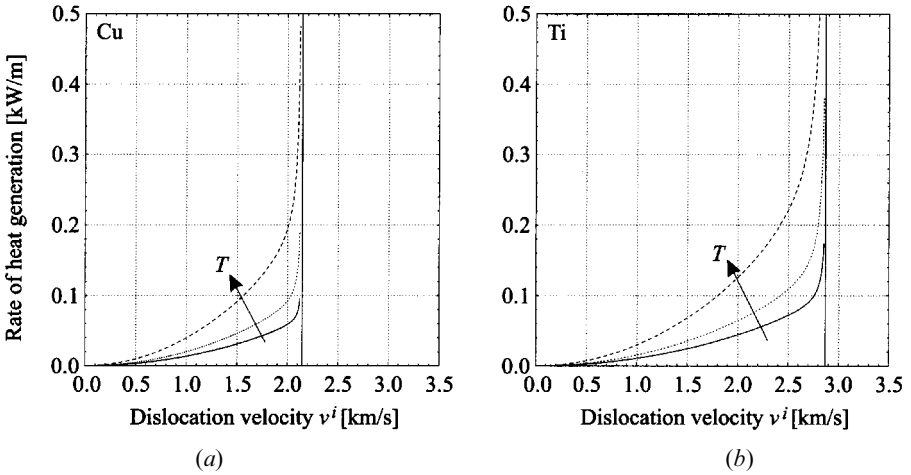

(*a*) (*b*)

Figure 3. Rate of heat generation per unit length due to a dislocation moving at a velocity $0 \leqslant v \leqslant a_2$ for (*a*) Cu (lines converging to $a_2 = 2.1\,\mathrm{km\,s^{-1}}$) and (*b*) Ti (lines converging to $a_2 = 2.9\,\mathrm{km\,s^{-1}}$): (——), ambient temperature of 100 K; (· · · · · ·), ambient temperatur of 298 K; (- - - -), ambient temperature of 900 K.

$$\Im(\varepsilon_{12})(\mathbf{q}) = \mathrm{i}\left(\frac{2}{\pi}\right)^{1/2} \frac{\delta(q_3)\exp(-\mathrm{i}q_1 v t)ba_2^2}{v^2}\left(\frac{-\beta_1^2 q_2}{q_2^2+\beta_1^2 q_1^2}+\frac{\alpha^4 q_2}{q_2^2+\beta_2^2 q_1^2}\right). \tag{9}$$

With a_1 and a_2 the longitudinal and shear wave velocities, respectively, α, β_1 and β_2 are defined as

$$\alpha = \left(1-\frac{v^2}{2a_2^2}\right)^{1/2}, \quad \beta_1 = \left(1-\frac{v^2}{a_1^2}\right)^{1/2}, \quad \beta_2 = \left(1-\frac{v^2}{a_2^2}\right)^{1/2}. \tag{10}$$

It agrees rather well with the empirical relation of Gillis *et al.* (1969). The heat generated during one time increment k can now be written as (using the Peach–Koehler equation $\sigma_{PK} b = B_{TOT}(v)v$)

$$\dot{q}_k = B^0_{wind} v^2 + \frac{B^0_{flut} v^2}{1-(v/a_2)^2}. \tag{11}$$

The rate of generation is plotted in figure 3.

§4. Solutions of the heat equation

The temperature rise ΔT due to the moving dislocations can be found using an analytical approach, or through a numerical analysis using finite-element techniques. Because of the nature of the problem, which may result in a rapidly varying temperature field, both methods are developed and compared in terms of computational speed and accuracy. This dualistic approach also provides a means of checking the consistency of both solutions.

The analytical solution will be developed in this section. The equations will be developed with the computational set-up of the previous sections (figure 2) in mind. Thus, the production of heat is provided by moving dislocations in a two-dimensional rectangular computational cell of width $\times$ height $= 2w \times 2h$, which is periodic in the x_1 direction and bounded at $x_2 = \pm h$. The time integration takes place in discrete time increments k, during which the dislocation velocities v_k (and, consequently, the source strengths q_k) are constants. At time increment $k = 0$, that is before any deformation, the computational cell is assumed to be in thermal equilibrium and $T_{k=0} \equiv T_0$ is constant everywhere. The duration of the time increments is fully controlled by the mechanical part of the simulation. The maximum possible length of these time increments is sufficiently small to ensure the stability of the thermal solution.

Green's functions are among the standard tools of finding an analytical solution of the heat equation. When applied to two-dimensional thermal problems, the Green's function $u(x_1, x_2, x_1', x_2', t, t')$ denotes 'the temperature at (x_1, x_2) at the time t due to an instantaneous line source of strength unity generated at the point $P(x_1', x_2')$ at the time t', the solid being initially at zero temperature, and the surface being kept at zero temperature'. In our specific case with discrete time increments, the initial temperature corresponds to the temperature at the start of a certain time increment k (i.e. at t_k). Given the temperature at t_k, the task at hand is to find the temperature at the end of the time increment, which corresponds to the start of time increment $k+1$ (i.e. at t_{k+1}).

Tailoring the expression of De Hosson (2000) to our specific case, the solution of the temperature field $T(x_1, x_2, t_{k+1})$ for a surface temperature $T_s(x_1, x_2, t)$ and initial internal temperature $T(x_1, x_2, t_k)$ and an internal heat source $\dot{q}_k(x_1, x_2, t)$

$$T(x_1, x_2, t_{k+1}) = \iint u_{t'=t_k} T(x_1', x_2', t_k)\, dx_1'\, dx_2' + \kappa \int_{t_k}^{t_{k+1}} \left(- \int T_s(x_1', x_2', t')\, \frac{\partial u_{t=t_{k+1}}}{\partial n}\, ds + \iint \frac{\dot{q}_k}{K}\, u_{t=t_{k+1}}\, dx_1'\, dx_2' \right) dt'. \tag{12}$$

The integration in the second term on the right-hand side is carried out over the top and bottom surfaces, and the differentiation is along the inward normal n of the respective surfaces. At all times, there is no heat exchange with the environment, that is the whole process is assumed to be adiabatic. In mathematical terms, this means enforcing

$$\frac{\partial u_k}{\partial n} = 0, \tag{13}$$

at the top and bottom boundaries, causing the second term on the right-hand side of equation (12) to vanish, and we are left with

$$T(x_1, x_2, t_{k+1}) = \iint u_{t'=t_k} T(x_1', x_2', t_k)\, dx_1'\, dx_2' + \kappa \int_{t_k}^{t_{k+1}} \iint \frac{\dot{q}_k}{K}\, u_{t=t_{k+1}}\, dx_1'\, dx_2'\, dt'. \tag{14}$$

The development of the temperature at zero initial temperature and zero flux across the surface is straightforward but cumbersome. The Green's function $u(x_1, x_2, x_1', x_2', t, t')$ for a unit line source at (x_1', x_2') in the computational cell of figure 2 for $t > t'$ equals

$$\frac{\exp\left[(x_1 - x_2')^2 / 4\kappa(t - t')\right]}{4h[\pi\kappa(t - t')^{1/2}]} \left\{ 1 + 2 \sum_{m=1}^{\infty} \exp\left(\frac{\kappa m^2 \pi^2 (t - t')}{4h^2} \right) \times \cos\left[\frac{m\pi}{2} \left(\frac{x_2}{h} + 1 \right) \right] \cos\left[\frac{m\pi}{2} \left(\frac{x_2'}{h} + 1 \right) \right] \right\}. \tag{15}$$

Note that equation (15) fulfils requirement (13). The summation over m arises owing to the finite extent of the computational cell in the (vertical) x_2 direction. For fast numerical convergence, one may convert equation (15) to a summation involving exponentials using Poisson's summation formula (Carslaw and Jäger 1959).

During the same increment k, the sources are described by taking into account all dislocations $n_{DIS}(k)$ and their replicas n:

$$\dot{q}_k = \sum_{i=1}^{n_{DIS}(k)} \sum_{n=-\infty}^{\infty} \dot{q}_k^i\, \delta(x_1' - [x_1^i + 2nw + v_k^i (t - t_k)], x_2' - x_2^i). \tag{16}$$

The contribution to the temperature rise $T(x_1, x_2, t_{k+1})$ due to the moving sources in time increment k is found by carrying out the integrations in the second term on the right-hand side of equation (14). The result is a temperature rise $T(x_1, x_2, t_{k+1})$ of

$$\sum_{i=1}^{n_{DIS}(k)} \sum_{n=-\infty}^{\infty} \frac{\dot{q}_k^i \exp(-2ZX)}{2\rho c_v h \kappa^{1/2}} \left\{ \frac{1}{2|Z|} \left[\exp(-2|XZ|)\,\mathrm{erfc}\left(\frac{|X| - |Z|\,\Delta t_{k+1}}{(\Delta t_{k+1})^{1/2}} \right) \right.\right.$$

$$\left. - \exp(2|XZ|)\,\mathrm{erfc}\left(\frac{|X| + |Z|\,\Delta t_{k+1}}{(\Delta t_{k+1})^{1/2}} \right) \right]$$

$$+ \sum_{m=1}^{\infty} \frac{1}{|Y|} \cos\left[\frac{m\pi}{2} \left(\frac{x_2}{h} + 1 \right) \right] \cos\left[\frac{m\pi}{2} \left(\frac{x_2^i}{h} + 1 \right) \right]$$

$$\left. \times \left[\exp(-2|XY|)\,\mathrm{erfc}\left(\frac{|X| - |Y|\Delta t_{k+1}}{(\Delta t_{k+1})^{1/2}} \right) - \exp(2|XY|)\,\mathrm{erfc}\left(\frac{|X| + |Y|\Delta t_{k+1}}{(\Delta t_{k+1})^{1/2}} \right) \right] \right\}, \tag{17}$$

with

$$X_k^i(n) \equiv \frac{x_1 - x_1^i - 2nw - v_k^i\,\Delta t_{k+1}}{(4\kappa)^{1/2}}, Y_k^i(m) \equiv \frac{|v_k^i|}{(4\kappa)^{1/2}} \left[1.0 + \left(\frac{\pi\kappa m}{v_k^i h} \right)^2 \right]^{1/2}, \tag{18}$$

$$Z_k^i \equiv \frac{v_k^i}{(4\kappa)^{1/2}}. \tag{19}$$

In equation (17), the indices *i, k, n* and m have partly been dropped. Now that we have obtained the second term on the right-hand side of equation (14), we focus our attention to the first term. The initial temperature field at time increment k equals the temperature field of the previous time increment $k-1$. The temperature field at the first increment is taken to be constant, that is $T(x_1, x_2, t_0) = T_0$. During the first time increment $k = 0$, the diffusion term again yields T_0, as one would expect. The temperature rise (17) has been plotted in figures 4 and 5, for Cu, Al and Ti and at low (figure 4) and high (figure 5) dislocation velocities.

For $k = 1$, the result is based on an evaluation of the actual values of X_k^i, Y_k^i and Z_k^i for Cu and Ti. Introducing

$$\beta_1^- = \frac{X_0^i + |Z_0^i|\,\Delta t_1 - (Z_0^i - |Z_0^i|)\,\Delta t_2}{(\Delta t_1)^{1/2}}, \qquad \beta_2^- = \frac{X_0^i + |Y_0^i|\,\Delta t_1 - (Z_0^i - |Y_0^i|)\,\Delta t_2}{(\Delta t_1)^{1/2}},$$

$$\beta_1^+ = \frac{-X_0^i + |Z_0^i|\,\Delta t_1 + (Z_0^i + |Z_0^i|)\,\Delta t_2}{(\Delta t_1)^{1/2}}, \quad \beta_2^+ = \frac{-X_0^i + |Y_0^i|\,\Delta t_1 + (Z_0^i + |Y_0^i|)\,\Delta t_2}{(\Delta t_1)^{1/2}}, \tag{20}$$

and with time steps in the range between 10^{12} and 10^{-9} (around the Debye frequency) the integration leads to a temperature rise $T(x_1, x_2, t_2)$ of

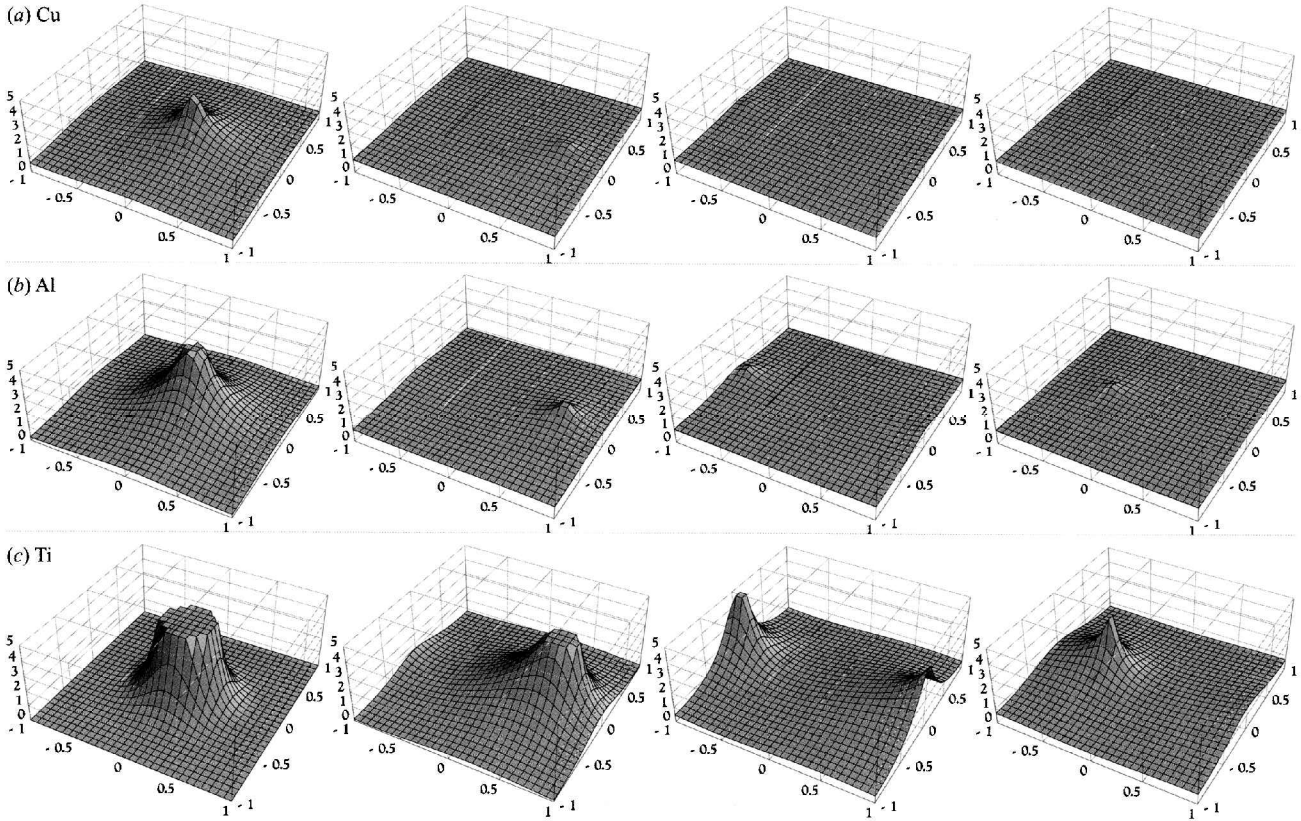

Figure 4. The temperature rise of equation (17) at different times for (*a*) Cu, (*b*) Al and (*c*) Ti. The velocities and source strengths of the dislocations have been given the same value. All pictures have been normalized to the average temperature rise of the computational cell. The temperature field was calculated in a computational cell of $2w \times 2h = 2\,\mu\text{m} \times 2\,\mu\text{m}$ and an 800×800 mesh. The time difference between each picture is 20 ns. The dislocation velocity is $25\,\text{m}\,\text{s}^{-1}$ and the source strengths are $18\,\text{mW}\,\text{m}^{-1}$.

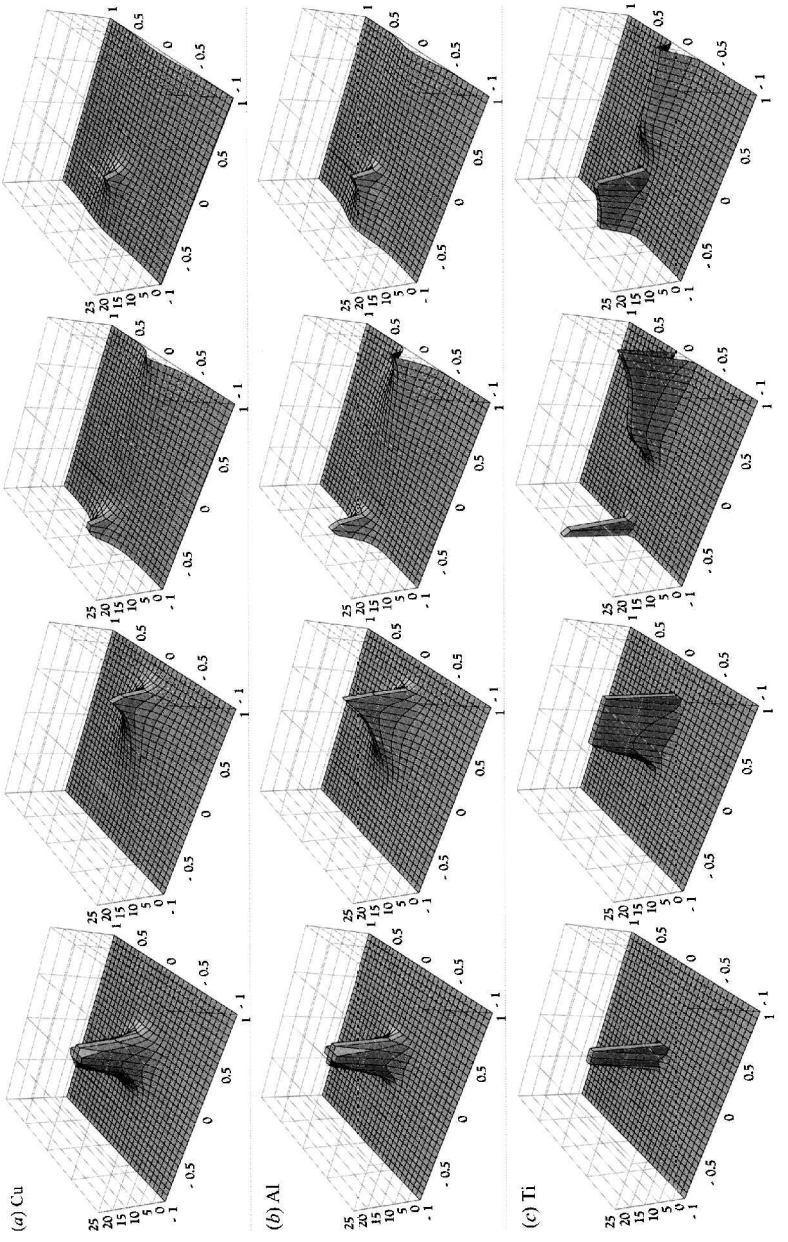

Figure 5. The temperature rise of equation (17) at different times for (*a*) Cu, (*b*) Al and (*c*) Ti. The velocities and source strengths of the dislocations have been given the same value. All pictures have been normalized to the average temperature rise of the computational cell. The temperature field was calculated in a computational cell of $2w \times 2h = 2\,\mu\text{m} \times 2\,\mu\text{m}$ and 800×800 mesh. The velocity is chosen to be half the shear wave velocity in Cu ($1072\,\text{m s}^{-1}$). The time difference between each picture (0.45 ns) has been chosen such that the positions are identical with those in figure 4. The source strengths are $150\,\text{W m}^{-1}$.

$$\sum_{i=1}^{n_{DIS}(0)} \sum_{n=-\infty}^{\infty} \frac{\dot{q}_0^i}{4\rho c_v h|v_0^i|}$$
$$\times \left(\left\{ \left(\frac{\Delta t_1}{\Delta t_2} \right)^{1/2} \left[\exp\left[(Z_0^i + |Z_0^i|)^2 \, \Delta t_2 - 2(Z_0^i + |Z_0^i|) X_0^i \right] \right. \right.$$
$$\times \operatorname{erf}\left(\frac{X_0^i - (Z_0^i + |Z_0^i|)\, \Delta t_2}{(\Delta t_2)^{1/2}} \right)$$
$$- \exp\left[(Z_0^i - |Z_0^i|)^2 \, \Delta t_2 - 2(Z_0^i - |Z_0^i|) X_0^i \right] \operatorname{erf}\left(\frac{X_0^i - (Z_0^i - |Z_0^i|)\, \Delta t_2}{(\Delta t_2)^{1/2}} \right) \Bigg]$$
$$+ \{ \operatorname{sgn}(\beta_1^-) \exp\left[(Z_0^i - |Z_0^i|)^2 \Delta t_2 - 2(Z_0^i - |Z_0^i|) X_0^i \right]$$
$$\left. + \operatorname{sgn}(\beta_1^+) \exp\left[(Z_0^i + |Z_0^i|)^2 \, \Delta t_2 - 2(Z_0^i + |Z_0^i|) X_0^i \right] \} \right\}$$
$$+ \sum_{m=1}^{\infty} 2 \exp\left(\frac{\kappa m^2 \pi^2 \, \Delta t_2}{4h^2} \right) \cos\left[\frac{m\pi}{2} \left(\frac{x_2}{h} + 1 \right) \right]$$
$$\times \cos\left[\frac{m\pi}{2} \left(\frac{x_2^i}{h} + 1 \right) \right] \Bigg/ \left[1 + \left(\frac{\pi \kappa m}{v_0 h} \right)^2 \right]^{1/2}$$
$$\times \left(\frac{\Delta t_1}{\Delta t_2} \right)^{1/2} \left[\exp\left[(Z_0^i + |Y_0^i|)^2 \, \Delta t_2 - 2(Z_0^i + |Y_0^i|) X_0^i \right] \operatorname{erf}\left(\frac{X_0^i - (Z_0^i + |Y_0^i|)\, \Delta t_2}{(\Delta t_2)^{1/2}} \right) \right.$$
$$- \exp\left[(Z_0^i - |Y_0^i|)^2 \, \Delta t_2 - 2(Z_0^i - |Y_0^i|) X_0^i \right] \operatorname{erf}\left(\frac{X_0^i - (Z_0^i - |Y_0^i|)\, \Delta t_2}{(\Delta t_2)^{1/2}} \right) \Bigg]$$
$$+ \left\{ \operatorname{sgn}(\beta_2^-) \exp[(Z_0^i - |Y_0^i|)^2 \, \Delta t_2 - 2(Z_0^i - |Y_0^i|) X_0^i] \right.$$
$$\left. \left. + \{ \operatorname{sgn}(\beta_2^+) \exp\left[(Z_0^i + |Y_0^i|)^2 \Delta t_2 - 2(Z_0^i + |Y_0^i|) X_0^i \right] \} \right\} \right). \tag{21}$$

In conclusion, the temperature rise at a particular location within the slab due to a set of moving dislocations in a time interval can be expressed (in a more or less) analytical form, at least for the first two time increments. In principle this is also possible for later time increments, but the equations become too complex to be presented explicitly.

§ 5. Thermal plasticity

In the following section, the computational set-up as developed in the previous sections is applied to fast deformation of the computational cell. First, some simulations at different but constant ambient temperatures will be carried out, in order to see the effects of the now temperature-dependent obstacle strengths and drag coefficients. In these cases, the heat equation does not enter the simulations yet. In § 5.2, however, the heat equation will be solved for a particular case. The analytical solution will be compared with the solution provided by the finite-element method as a mutual validation. The differences in localization of heat will be studied, along the same lines as in figures 4 and 5.

5.1. *Discrete dislocation plasticity at constant ambient temperature*

This section presents a set of simulations showing the effect of the ambient temperature on the deformation behaviour of the computational cell. Two realizations of the same initial parameters of Al are subjected to an applied strain rate $\gamma = 10^6\,s^{-1}$ at ambient temperatures of 100, 298 and 900 K, up to a shear strain of 2.5%. The microstructural set-up corresponds to that described by Roos *et al.* (2000). Figure 6 displays an example of the initial configuration of the computational cell of figure 2, including the slip planes, obstacles, nucleation sites and a random distribution of dislocations. The cell contains solutes with an atomic fraction $c = 5 \times 10^{-4}$, forest dislocations with a strength $f_c = 10^{-3}$ and a fixed fraction $f_F = 10^{-2}$ of the mobile dislocation density.

The resulting shear stress–shear strain curves are presented in figure 7. The figures display a trend of increasing flow stress with increasing temperature. At a strain rate of $10^6\,s^{-1}$, the temperature dependence of the deformation lies in the temperature dependence of the drag coefficient. The thermal softening of obstacles is rendered ineffective above strain rates of the order of 10^3-$10^4\,s^{-1}$, in accordance with the discussion at the end of §2. In fact, according to equation (5) the drag coefficient increases linearly with increasing temperature, and the variation in flow stress at constant dislocation density should reflect this dependence. In the curves in figure 7(*b*) the final dislocation densities approach the same constant values; at $\gamma = 2.5\%$, $\rho_{TOT} = 2.6 \times 10^{13}\,m^{-2}$ for realization 1 at all temperatures, and

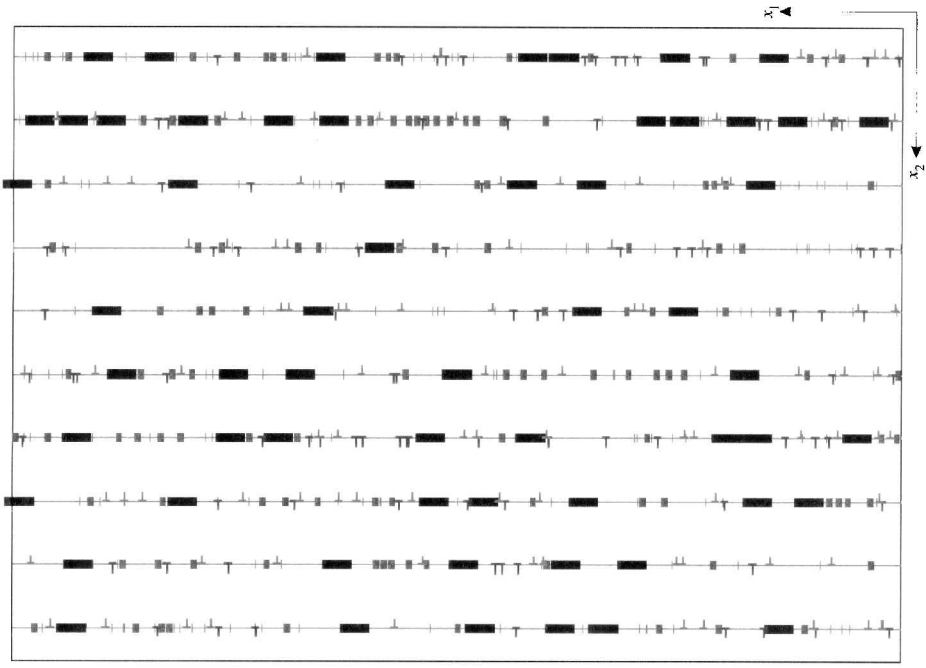

Figure 6. Example of the initial configuration in the computational cell (rotated 90° and stretched in the x_1 direction). The computational cell of $2w \times 2h = 2\,\mu m \times 2\,\mu m$ contains ten horizontal slip planes (grey). The cell contains dislocations (positive, red; negative, green), nucleation sites (blue), precipitates (magenta) and solutes and forest dislocations (orange). The parameters that were used to generate this particular configuration are given in the text.

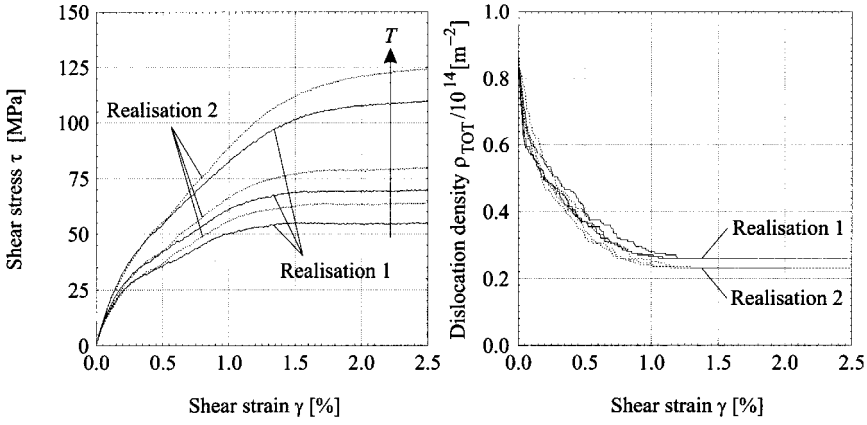

(*a*) (*b*)

Figure 7. Effect of different ambient temperatures in Al for two different realizations of the same initial conditions, where the computational cell is deformed at a strain rate $\dot{\gamma} = 10^6\,s^{-1}$: (——), realization 1; (· · · · ·), realization 2. (*a*) Shear stress versus shear strain. The lines ending from low to high final shear stress correspond to temperatures of 100, 298 and 900 K respectively. (*b*) Total dislocation densities.

$\rho_{TOT} = 2.3 \times 10^{13}\,m^{-2}$ for realization 2 at all temperatures and the curves in the left figure 7 are consistent with this interpretation.

5.2. *Consistency of analytical and finite-element solutions*

In this section, the solutions of the analytical expressions in the previous section are compared with a finite-element solution. To this end, similar runs to those for as figures 4 and 5 have been carried out for both methods. In a periodic box of $2w \times 2h = 2\,\mu m \times 2\,\mu m$, one dislocation is put on a slip plane at $x_2 = 0$. The temperature fields are calculated at four distinct times $t_1 = 0.12\,ns$, $t_2 = 0.58\,ns$, $t_3 = 1.05\,ns$ and $t_4 = 1.52\,ns$. The dislocation velocity is constant at $v = \frac{1}{2}a_2^{Cu}$ throughout the simulations, so that the analytical expression (17) can be used. Similarly, the rate of heat generation is kept constant at $150\,W\,m^{-1}$ (i.e. not according to equation (17)). The summation over m in equation (17) is carried out for m up to 500. The summation over n runs from -10 to 10.

In the finite-element formulation (Zienkiewicz and Taylor 1967, Cook 1995) of the thermal problem, the temperature field is approximated on bilinear rectangular elements. The computational cell (figure 2) is divided into a grid of 400×400 rectangular elements The elements are assumed to be isotropic. The finite element formulation of equation (6) is solved by the slightly overdamped Galerkin method to ensure the numerical stability during short time increments. The heat emanating from the moving dislocations (equation (11)) is properly distributed over the appropriate nodes (Metselaar *et al.* 2000).

At $x_2 = 0$, a cut is made through the computational cell, and the temperature fields due to the dislocation moving along $x_2^{DIS} = 0$ are compared along this cut. The results are displayed in figure 8 (*a*) for Cu. A similar run is carried out where the dislocation is now placed on a slip plane at $x_2^{DIS} = -4h/7$, in order to avoid cancellation of errors due to the symmetry of the previous run. The cut along

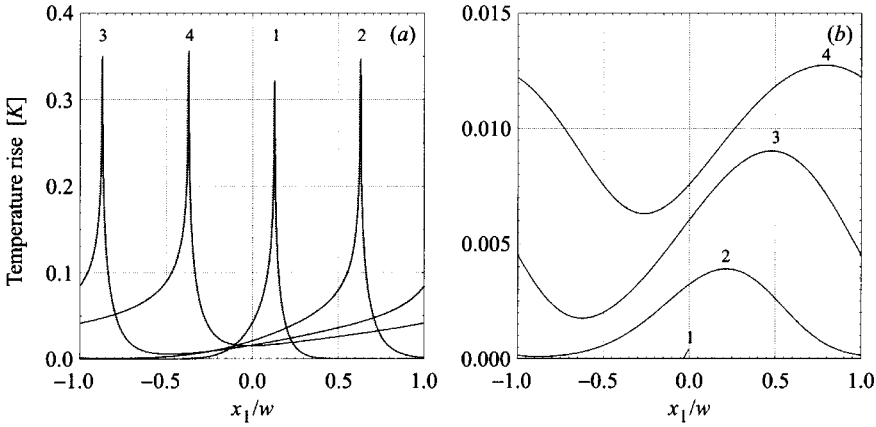

Figure 8. Comparison of analytical solution (——) and finite element solution (· · · · · ·) of the heat equation in Cu (both solutions are so close together that the solid and dotted curves are hardly visible separately). The numbers in the graphs correspond to the subscripts of the time increments. The comparison was taken along the horizontal line (*a*) $x_2 = 0$ for $x_2^{\mathrm{DIS}} = 0$ and (*b*) $x_2 = 3h/200$ for $x_2^{\mathrm{DIS}} = -4h/7$.

which the temperature fields are compared now is at $\mathrm{x}_2 = 3\mathrm{h}/200$. The result is displayed in figure 8 (*b*). From these graphs we conclude that the analytical solutions and the finite-element solution of § 4 are consistent with one another. Furthermore, the finite-element method may safely be used to calculate the temperature rise in more complex configurations, where the analytical solutions become too complex to be used in practice.

5.3. *Localization of heat*

Now that the consistency between the analytical solution and the finite-element solution is confirmed, it is possible to calculate the temperature rise due to fast deformation of the computational cell. First, the differences between the localization in Al and Ti are studied. To that end, two simulations are carried out with identical initial configurations, identical deformation rates, etc. So far, only the initial constant temperature is taken into account in the mechanical part. The only difference is in the thermal conductivities and the specific heats. In figure 9 the normalized temperature rise is displayed during deformation ($\gamma = 10^6\,\mathrm{s}^{-1}$) of Al (figures 9 (*a*) and (*c*)) and Ti (figures 9 (*b*) and (*d*)) at different stages of the deformation. The temperature field was calculated in a computational cell of $2\mathrm{w} \times 2\mathrm{h} = 2\,\mu\mathrm{m} \times 2\,\mu\mathrm{m}$ and a 800×800 mesh.

The average temperature rise for both metals lies in the same range: between 10 and 20 K at a shear strain of 7.5%. Figure 9 clearly shows the stronger localization in Ti with respect to Al (note the difference in scale). The slip is concentrated in a few glide planes, and this is reflected in the temperature fields, especially in the case of Ti. At later times, these differences become smaller, as the generated heat has had more time to diffuse throughout the computational cell.

The fact that the temperature rise in ordinary slip is only of the order of 10–20 K implies that the effect on the flow stress in the fully coupled case will be negligible. It is also consistent with the observation that for normal slip the temperature rise is not nearly high enough to induce melting. The present simulations show that the same

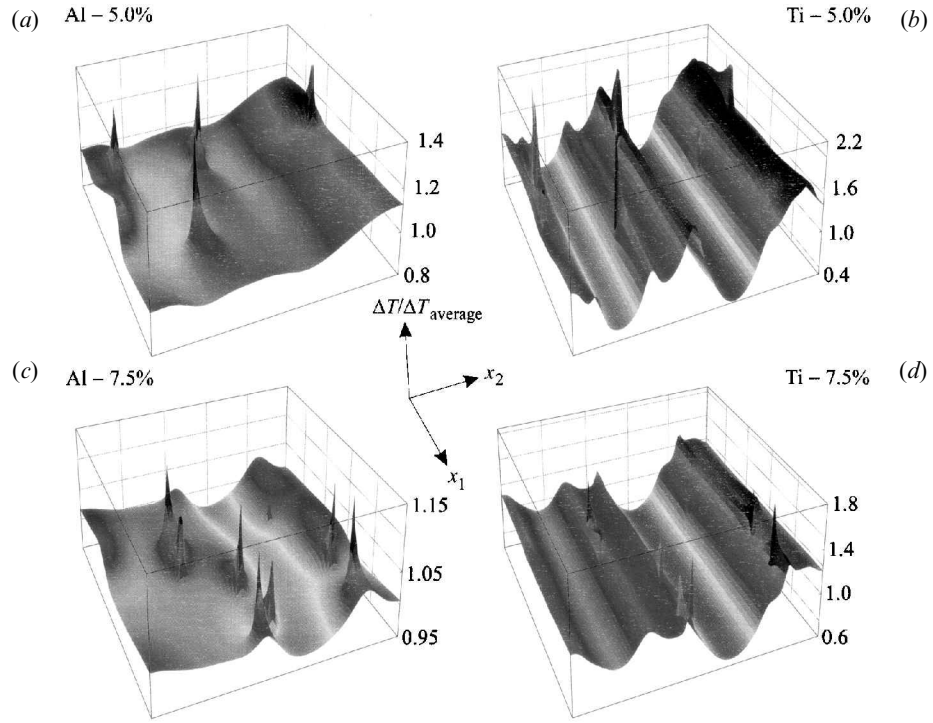

Figure 9. Effect of bulk thermal properties on the temperature rise in Al ((*a*) $\gamma = 5\%$ and $\Delta T_{\text{average}} = 4.0\,\text{K}$; (*c*) $\gamma = 7.5\%$ and $\Delta T_{\text{average}} = 13.6\,\text{K}$) and Ti ((*b*) $\gamma = 5\%$ and $\Delta T_{\text{average}} = 4.3\,\text{K}$; (*d*) $\gamma = 7.5\%$ and $\Delta T_{\text{average}} = 14.5\,\text{K}$). The coordinates in the bottom plane denote the position in the computational cell, where the horizontal planes lie along the x_1 direction. The temperature fields are normalized with respect to their *average* temperature rise $\Delta T_{\text{average}}$. The two simulations have identical initial configurations.

conclusion holds at the high strain rate of $10^6\,\text{s}^{-1}$, even in Ti, which has a strong thermal localization. These results can be compared with prediction based on a macroscopic description of a homogeneously strained material. The temperature rise induced by mechanical work up to a certain strain γ_F can simply be equated to

$$\Delta T = \frac{\xi}{\rho c_p} \int_0^{\gamma_F} \tau \, d\gamma, \tag{22}$$

where ξ is the fraction of mechanical work converted into heat, ρ the material density and c_p the specific heat at constant pressure. Substitution of the constitutive equation proposed by Johnson *et al.* (1983) leads (for m = 1 and B and C constants) to

$$\Delta T = (T_m - T_R)\left\{1 - \exp\left[\frac{-\xi[1 + C \ln(\dot{\gamma}/\dot{\gamma}_0)]}{\rho c_p (T_m - T_R)}\left(\tau_0 \gamma_F + \frac{B\gamma_F^{n+1}}{n+1}\right)\right]\right\}. \tag{23}$$

With the corresponding physical parameters for Al and Cu, plots of the temperature rise as a function of strain for various strain rates and τ_0 are displayed in figures 10 and 11 respectively. These are similar to the results from De Andrade *et al.* (1994), although their results are erroneous because of mistakes in the actual strain values.

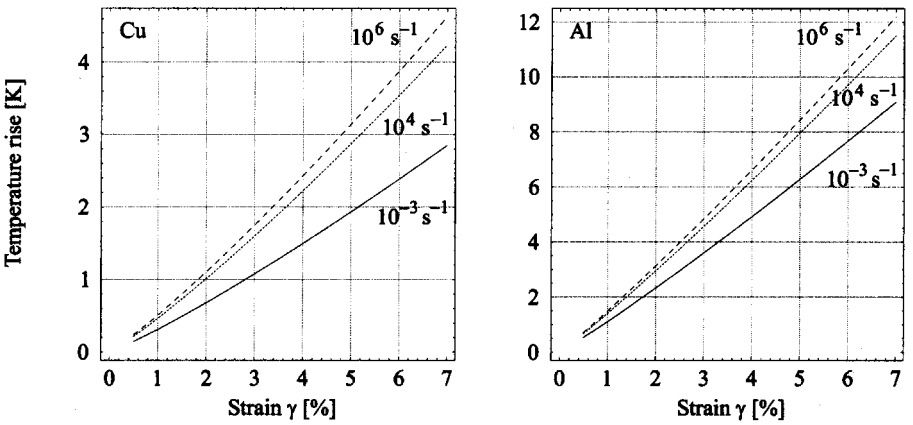

Figure 10. Temperature rise in (*a*) Cu and (*b*) Al according to equation (27), for different strain rates. In both cases, $T_R = 300$ K, $\dot{\gamma}_0 = 1\,s^{-1}$ and $\xi = 0.9$. For Cu, $B = 292$ MPa, $C = 0.025$, $\tau_0 = 90$ MPa and $n = 0.31$. For Al, $B = 426$ MPa, $C = 0.015$, $\tau_0 = 265$ MPa and $n = 0.34$.

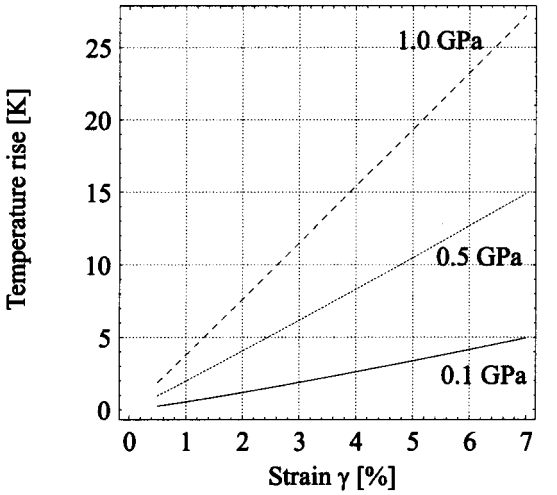

Figure 11. Temperature rise according to equation (27) in Cu at a *fixed* strain rate $\dot{\gamma} = 10^4\,s^{-1}$: (——), $\tau_0 = 0.1$ GPa; (· · · · · ·), $\tau_0 = 0.5$ GPa; (- - - -), $\tau_0 = 1.0$ GPa. Otherwise, the parameters are the same as in figure 10.

Here, ξ was taken to be 0.9 and the strain rate varies between 10^{-3} and 10^6. In accordance with the DDP calculations the temperature rise lies in the range of a few kelvins, somewhat higher for Al than for Cu. Even at a high yield stress τ_0 and deformation at high strain rates ($10^4\,s^{-1}$), the temperature rise is predicted to be around 25 K. At any rate, the present method of DDP is in accordance with macroscopic model predictions and it may also very well be able to predict the temperature rise due to a *catastrophic avalanche of a dislocation pile-up*. Therefore, we turn to crack propagation because experimentally a temperature increase up to the melting point is observed in a Ti alloy.

One mechanism that might give the proper order of magnitude is the propagation of a crack (Rice and Levy 1969). This makes sense, because after all, the molten material is observed on the fracture surface of Ti alloys. We start with equation (6) and identify the heat source term $\dot{q}_v(x_1, x_2, t)$ as the plastic work rate. Further, we assume that the energy dissipation is not uniform in the material but occurs non-uniformly in a restricted region around the moving crack. The maximum temperature rise is for a Dugdale (1960) crack given by

$$\Delta T_{max} = 2^{1/2} \frac{(1-\nu) K_{stress} \tau_0 v_{CRACK}^{1/2}}{2\mu(\rho c k)^{1/2}} \qquad \text{for} \qquad \frac{v_{CRACK}\omega}{2\kappa} \to \infty, \tag{24}$$

with k the thermal conductivity, K_{stress} the stress intensity factor and ω the plastic zone according to Dugdale (1960). This analysis indicates that for a given stress intensity factor the temperature rise is proportional to $v_{CRACK}^{1/2}$. The actual value depends also on the yield stress and the stress intensity factor. In figure 12 the temperature rises of various materials are plotted as functions of the normalized crack velocity. The stress intensity factors and the yield stresses, all at room temperature, were taken to be constant (from the literature). In contrast with the findings of the temperature rise due to dislocation motion, it is striking to see that upon crack propagation a far higher temperature rise is predicted. Beside thermal dissipation by crack propagation, there may also exist cooling ahead of the crack tip because of thermoelastic effects (Nye 1969). If the entropy of an elastic solid is supposed to remain constant, the cooling ahead of the crack can easily be calculated under the assumption that for an isotropic material the specific heat at constant stress is about equal to the specific heat at constant pressure. The predicted thermo-elastic cooling effect appears to be of minor importance which is in agreement with experiments on metallic glasses (Flores and Dauskardt 1999). Similarly it can be shown that the cooling in front of a moving (edge) dislocation is also just of the order of 1 K.

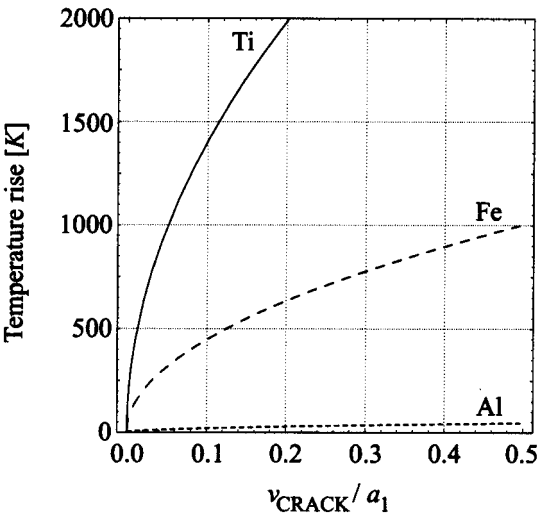

Figure 12. Temperature rise as a function of the crack velocity for Al, Fe and Ti for a Dugdale crack ($K_{cast\,Al} = 22\,MPa\,m^{1/2}$; $K_{low\,alloy\,steel} = 55\,MPa\,m^{1/2}$; $K_{Ti\,alloy} = 55\,MPa\,m^{1/2}$) (equation (24)).

With the DPP approach it is possible to scrutinize to a greater depth the crack propagation. Because dislocations represent discontinuities in displacement, they can also describe a macroscopic crack, at least in a mathematical sense (Eshelby *et al.* 1951, Leibfried 1951, Weertman 1996). To unravel the basic concepts for dynamic crack propagation, the DDP approach may prove itself useful. In particular it is important to understand the dynamic stress intensity factor. The reason for this can be illustrated by studying equation (24) again. In a macroscopic sense, the critical stress intensity factor increases upon increasing temperature. However, usually the toughness decreases also with increasing loading rate. The latter effect is commonly attributed to the fact that the effective yield stress is rate dependent whereas the stress level for fracture is essentially independent of the loading rate. Consequently, the loading rate itself and the local temperature rise at the crack tip with increasing loading rate have opposing effects. We may speculate about the existence of a critical loading rate above which the critical stress intensity factor is not a function of the loading rate any longer and only in that situation would the temperature rise become the determining factor (Rice 1968). If the strain-rate sensitivity is small, for instance in a Ti alloy, this critical loading rate effect is probably quite small and an effect of the local temperature rise on the increase in toughness is already expected at lower loading rates. In addition, with increasing local temperature the term $\rho c_p k$ decreases and therefore the temperature rise in equation (24) becomes a lower bound. In principle the DDP can include inertia effects, that is those for dynamic crack propagation. The question remains whether the velocity dependent drag coefficients of a single dislocation can be easily transferred to the velocity dependent drag coefficient of a moving crack. As a first approximation the drag coefficient of the moving crack can be set equal to the drag coefficient of a moving pile-up of superlattice dislocations, but these aspects have to be investigated further.

Only recently a discrete analysis of mode-I crack growth was carried out (Cleveringa *et al.* 2000). There, the fracture properties of a material are based on a cohesive surface constitutive equation and plastic flow occurred by a collective motion of discrete dislocations. From this analysis, it is interesting to note that the fracture behaviour depends very sensitively on the density of pre-existing dislocation sources around the crack. At a low density, only isolated dislocations are generated, leading to brittle failure. At a high density of dislocation sources, a continuous crack tip blunting without crack propagation is observed. Certainly, when one considers fracture at high strain rate deformation, the dynamics should be properly incorporated. The analysis should not be solely based on a stationary crack that emits dislocations, as is usually done in the literature. It is feasible that a stationary crack may emit dislocations, whereas a fast moving crack will only nucleate dislocations that are not moving at a velocity high enough to escape from the stress field of the moving crack. In such a situation, although dislocations are nucleated, indeed they will not necessarily contribute to a relaxation of the (cleavage) fracture stress. The intrinsically ductile failure under stationary conditions may still exhibit brittle failure under dynamic conditions. Indeed, recent results of DDP simulations (Cleveringa *et al.* 2000) do suggest this, even though these calculations did not include full dynamic, that is inertia effects. Using a relatively simple model of the type used by Roberts (1996), Gumbsch (1996), Gumbsch and Cannon (2000) and Riedle *et al.* (1996) have explored some of these issues, again under quasistatic conditions and ignoring dissipative temperature changes. They also confirmed the above-mentioned sensitivity to pre-existing dislocations and the competition between

dislocation mobility and nucleation. Although these seem to be all-important aspects of dynamic fracture, to the best of our knowledge there have been only a few attempts known in the literature to tackle this question (Freund 1993) but even so not at the level of dislocations. Indeed it can be shown (Roos *et al.* 2000) that the acceleration of a dislocation including drag terms is extremely high and the time needed to bring the dislocation to a steady state velocity is very short. The dislocation will reach steady state velocity after it has travelled a very small distance, that is about 1% or even less of its mean slip distance. Consequently, the time interval and distance required to bring the dislocation to its steady-state situation is so small that in a physical description it can be neglected. This is in agreement with the conclusions of Gillis and Kratochvil (1970). However, this is certainly not the case for crack propagation and inertia effects should be investigated. In principle the DDP approach, including the local temperature effects as delineated in this paper, can be explored further in the future to elucidate these fundamental problems in dynamic fracture mechanics at high strain rate deformations.

§ 6. Conclusions

In this paper, the DDP method is extended to include explicitly the thermal effects of moving dislocations. In this manner, localization of heat during fast deformation can be calculated exactly. The thermal effects included are the thermal dissipation due to dislocation drag, the temperature dependence of the drag coefficients themselves and a temperature-dependent obstacle strength through a simple Arrhenius-type dependence. The temperature distribution is calculated using a time-dependent Galerkin finite-element solution. An analytical solution is also presented. The two solutions are compared to provide a mutual validation. The stress–strain curves are calculated for Al under simple shear for constant temperatures of 100, 298 and 900 K. The stress–strain curves reflect the temperature dependence of the drag coefficients, since the deformation takes place at a strain rate of $10^6\,s^{-1}$, which is well within the drag-controlled regime. Finally, the temperature distribution for Al and Ti are calculated. At 7.5% shear strain, the maximum temperature rise is of the order of 20 K in Ti. This is orders of magnitude lower than the melting temperature, the temperature which has experimentally observed to be reached. It is anticipated that this is caused by crack propagation which will be modelled by a DDP approach in future work.

Acknowledgements

The work described in this paper is supported by IOP metals under project C94.703.RG.TF and the Netherlands Institute for Metals Research under project MS97006. Thanks are due to Professor Erik van der Giessen for comments and many stimulating discussions.

References

Armstrong, R. W., and Elba, W. L., 1989, *Mater. Sci. Engng.,* **A122**, L1.

Carslaw, H. S., and Jäger, J. C., 1959, *Conduction of Heat in Solids,* second edition (Oxford: Clarendon).

Cerv, J., Landa, M., and Machová, A., 2000, *Scripta mater.,* **43**, 423.

Cleveringa, H. H. M., Van der Giessen, E., and Needleman A., 2000, *J. Mech. Phys. Solids,* **48**, 1133.

Coffey, C. S., 1984, *Inst. Phys. Conf. Ser.,* **70**, 519.

Cook, R. D., 1995, *Finite Element Modeling for Stress Analysis* (New York: Wiley) chapter 8.

De Abdrade, U. R., Meyers, M. A., Vecchio, K. S., and Chokshi, A. H., 1994, *Acta metall. mater.,* **42**, 3183.
De Hosson, J. Th. M., 1999, *Laser Surface Heat Treatment* (New York: Academic Press).
De Hosson, J. Th. M., Kanert, O., and Sleeswijk, A. W., 1983, *Dislocations in Solids,* Vol. 6, edited by F. R. N. Nabarro (Amsterdam: North Holland), p. 441.
Detemple, K., Kanert, O., De Hosson, J. Th. M., and Murty, K. L., 1995, *Phys. Rev.* B, **52**, 125.
Duesbery, M., 1989, *Dislocations in Solids,* Vol. 8, edited by F. R. N. Nabarro (Amsterdam: North-Holland), p. 67.
Dugdale, D. C., 1960, *J. Mech. Phys. Solids,* **8**, 100.
Eshelby, J. D., Frank, F. C, and Nabarro, F. R. N., 1951, *Phil. Mag.,* **42**, 351.
Eshelby, J. D., and Pratt, P. L., 1956, *Acta metall.,* **4**, 560.
Flores, K. M., and Dauskardt, R. H., 1999, *J. Mater. Res.,* **14**, 638.
Freudenthal, A. M., and Weiner J. H., 1956, *J. appl. Phys.,* **27**, 44.
Freund, L. B., 1993, *Dynamic Fracture Mechanics* (Cambridge University Press).
Gillis, P. P., Gilman, J. J., and Taylor, J. W., 1969, *Phil. Mag.,* **20**, 279.
Gillis, P. P., and Kratochvil, J., 1970, *Phil. Mag.,* **21**, 425.
Gruner, P., 1965, *Phys. Status sol.,* **12**, 679.
Gumbsch, P., 1996, *Z. Metall.,* **87**, 341.
Gumbsch, P., and Cannon, R., 2000, *Mater. Res. Soc. Bull.,* **25**, 15.
Horstemeijer, M. F., and Baskes, M. I., 1999, *Trans. ASME,* **121** 114.
Johnson, G. R., Hoegfeldt, J. M., Lindholm, U. S., and Nagg A., 1983, *J. Eng. Mater. Technol.,* **105**, 42.
Kirchner, H. O., Kubin, L. P., and Pontikis, V., (editors), 1996, *Computer Simulation in Materials science: Nano/meso/macroscopic Space and Time Scales*, NATO Advanced Study Institute Series, Series E, Vol. 308 (Dordrecht: Kluwer).
Kogure, Y., and Hiki, Y., 1975, *J. phys. Soc. Japan,* **38**, 471.
Leibfreid, G., 1951, *Z. Phys.,* **130**, 214.
Mason, J. J., Rosakis, A. J., and Ravichandran G., 1994, *Mech. Mater.,* **17**, 135.
Metselaar, E. D., Roos, A., De Hosson, J. Th. M., and Van der Giessen, E., 1999, *Mater. Res. Soc. Symp. Proc.,* **538**, 93; 2000, *Microstructure, Mechanical Properties and Processes,* Vol. 3, edited by Y. Bréchet (Weinheim: Wiley WCH), p. 78.
Nadgornyi, E., 1988, *Prog. Mater.,* **31**, 10.
Nye, J., 1969, *Physical Properties of Crystals* (Oxford University Press), p. 176.
Rice, J., 1968, *J. appl. Mech.,* **35**, 379.
Rice, J., and Levy, N., 1969, *Physics of Strength and Plasticity,* edited by A. Argon (Cambridge, Massachusetts: MIT Press), p. 277.
Riedle, J., Gumbsch, P., and Fischmeister, H. F., 1996, *Phys. Rev. Lett.,* **76**, 3594.
Roberts, S. G., 1996, *Computer Simulation in Materials Science: Nano/meso/macroscopic Space and Time Scales,* NATO Advanced Study Institute Series, Series E, Vol. 308, edited by H. O. Kirchner, L. P. Kubin and V. Pontikis (Dordrecht: Kluwer), p. 409.
Roos, A., and De Hosson J. Th. M., 2001, *Phys. Rev.* B (submitted).
Roos, A, De Hosson, J. Th. M., Cleveringa, H. H. M., and Van der Giessen, E., 1998, *Simulation of Materials Processing,* edited by H. Huetink and F. Baaijens (Rotterdam: Balkema), p. 303.
Roos, A., De Hosson, J. Th. M., and Van der Giessen, E., 2000, *Comput. Mater. Sci.,* **20**, 1, 26.
Van der Giessen, E., and Needleman A., 1995, *Modelling Simulation Mater. Sci. Engng.,* **3**, 689.
Vitek, V., 1974, *Cryst. Lattice Defects,* **1**, 5.
Weast, R. C., Astle, M. A., and Beyer W. H. (editors), 1984, *CRC Handbook of Chemistry and Physics,* 65th edition (Florida: Boca Raton, CRC Press).
Weertman, J., 1996, *Dislocation Based Fracture Mechanics* (Singapore: World Scientific).
Zienkiewicz, O. C., and Taylor, R. L., 1967, *The Finite Element Method,* Vol. 2, fourth edition (New York: McGraw-Hill).